

Hydrophobicity within the three-dimensional Mercedes-Benz model: Potential of mean force

Cristiano L. Dias,^{1,a)} Teemu Hynninen,^{2,3} Tapio Ala-Nissila,^{3,4} Adam S. Foster,^{2,3} and Mikko Karttunen⁵

¹*Departments of Biochemistry and Department of Molecular Genetics, University of Toronto, Toronto, Ontario M5S 1A8, Canada and Department of Physics, University of Toronto, Toronto, Ontario M5S 1A7, Canada*

²*Department of Physics, Tampere University of Technology, FI-33101 Tampere, Finland*

³*Department of Applied Physics and COMP CoE, Aalto University School of Science, FI-00076 Aalto, Espoo, Finland*

⁴*Brown University, Providence Rhode Island 02906-1843, USA*

⁵*Department of Applied Mathematics, The University of Western Ontario, London, Ontario N6A 5B7, Canada*

(Received 5 August 2010; accepted 21 December 2010; published online 11 February 2011)

We use the three-dimensional Mercedes-Benz model for water and Monte Carlo simulations to study the structure and thermodynamics of the hydrophobic interaction. Radial distribution functions are used to classify different cases of the interaction, namely, contact configurations, solvent separated configurations, and desolvation configurations. The temperature dependence of these cases is shown to be in qualitative agreement with atomistic models of water. In particular, while the energy for the formation of contact configurations is favored by entropy, its strengthening with increasing temperature is accounted for by enthalpy. This is consistent with our simulated heat capacity. An important feature of the model is that it can be used to account for well-converged thermodynamics quantities, e.g., the heat capacity of transfer. Microscopic mechanisms for the temperature dependence of the hydrophobic interaction are discussed at the molecular level based on the conceptual simplicity of the model. © 2011 American Institute of Physics. [doi:10.1063/1.3537734]

I. INTRODUCTION

Since 1970s the hydrophobic effect has been one of the most discussed topics in biophysics, particularly the solvation of proteins and small molecules and their interactions with surfaces. The hydrophobic effect is intimately related to the way living matter undergoes self-organization and how phenomena such as protein folding and denaturation occur.^{1–9} References 10–14 provide recent reviews of the topic. Tanford¹⁵ provides a lucid account of the history of the hydrophobic effect since its explanation in 1938 by Irving Langmuir and how it slowly became one of the cornerstones of protein science.

The hydrophobic interaction, i.e., the water-mediated attraction between nonpolar solutes, is related to the particular hydration properties of nonpolar surfaces. While water can form up to four H-bonds in its bulk environment, close to nonpolar solutes it is hindered from forming H-bonds in the direction of the solute. To avoid the energetic cost related to the loss of a H-bond, these water molecules tend to assume a *reduced number* of low energetic configurations where the formation of H-bonds is maximized. This reduced number of conformations accounts for a free energy of hydration that has a lower entropy as compared to bulk water. Using ice as an analogy, the low entropic regions around solutes were named “iceberg,” although it was noted already in the original 1945 work of Frank and Evans¹⁶ that this analogy should not be

taken literally: close to the solute water is *not* in its solid state but it is perturbed toward crystallinity.^{17–19}

To avoid the high entropic cost of hydration, nonpolar solutes aggregate in water. The hydrophobic interaction refers to the energetics of this association, which is characterized²⁰ by an increase in entropy when small solutes are separated by short distances (typically $r < 5 \text{ \AA}$), and an unfavorable free energy when at intermediate distances ($5 \text{ \AA} < r < 6 \text{ \AA}$). Recently, computer simulations have identified several nontrivial features of the hydrophobic interaction. For example, the heat capacity of a pair of nonpolar solutes in water depends on the distance separating them—being negative at short distances and unexpectedly positive at intermediate distances.^{21–24} Also, the hydrophobic interaction between clusters of nonpolar solutes has been shown to be nonadditive.^{23,25–27}

In this paper, our focus is on the qualitative temperature dependent features of the hydrophobic effect. We use the three-dimensional Mercedes-Benz model (3DMB) (Ref. 28) to describe water molecules. A previous version of the model dates back to the early 1970s (Refs. 29–31) and has recently been studied analytically and through computer simulations.^{32,33} The 3DMB model²⁸ reproduces many of the features of bulk water at ambient conditions: the maximum density in the liquid phase of water, the negative thermal expansion coefficient, and the minimum in the compressibility of real water. It has recently been used to study regelation, i.e., the melting of ice when subjected to high pressure and its refreezing once this pressure is lifted.³⁴ Here, we embed nonpolar solutes within 3DMB water and use Monte Carlo simulations to study structural and thermodynamic properties

^{a)} Author to whom correspondence should be addressed. Electronic mail: diasc@physics.mcgill.ca.

of these systems. Previous studies using the two-dimensional Mercedes-Benz model have shown that this method provides valuable information about the hydrophobic effect and its thermodynamics in the presence of small molecules and the denaturation of proteins.^{35–39}

The paper is organized as follows. The model and computational details are provided in Sec. II. Structural properties using radial distribution functions (RDFs) are given in Sec. III. Thermodynamic properties are described in Secs. IV–VI in which we analyze the system in terms of the potential mean force and study its temperature dependence and heat capacity. The microscopic mechanism is discussed in Sec. VII, and we finish with discussion and conclusions in Sec. VIII.

II. SIMULATIONS

The 3DMB model mimics the interaction between water molecules²⁸ through three explicit terms: directional H-bonds, isotropic van der Waals interactions, and a dihedral angle term. The competition between these terms accounts for the properties of water. Following our previous work on the 3DMB model,²⁸ energies are reported in terms of binding energy between H-bonds, i.e., ϵ_{HB} , and distances are given in units of the equilibrium distance between H-bonds, R_{HB} . Temperature is given in units of $|\epsilon_{\text{HB}}|/k_B$ and the Boltzmann constant k_B is set to 1. Pressure is given in units of $|\epsilon_{\text{HB}}|/R_{\text{HB}}^3$. We use a pressure of 0.2 since at this pressure the 3DMB model reproduces the thermodynamical features of water at ambient conditions.²⁸

Simulations are carried out in the isothermal–isobaric (*NPT*) ensemble. Unless otherwise stated, we sample eight nonpolar solutes embedded in a solution of 504 Mercedes-Benz (MB) particles. Solute molecules are described by a Lennard-Jones potential

$$U_{\text{LJ}}(r_{ij}) = 4\epsilon_{\text{LJ}} \left[\left(\frac{\sigma_{\text{LJ}}}{r_{ij}} \right)^{12} - \left(\frac{\sigma_{\text{LJ}}}{r_{ij}} \right)^6 \right], \quad (1)$$

with binding energy for solute–solute interactions set to $\epsilon_{\text{LJ}} = \epsilon_{\text{ss}} = 0.15$ and equilibrium distance to $R_{\text{LJ}} = 2^{1/6}\sigma_{\text{ss}} = 1.30$. The size of these solutes is comparable to Ar (for which $R_{\text{Ar}} = 1.88 \text{ \AA}$ and in units of the solvent radius $R_w = 1.4 \text{ \AA}$ gives $R_{\text{Ar}}/R_w = 1.34$) and methane ($R_{\text{methane}}/R_w = 1.35$).⁴⁰ For interactions between solute and MB water molecules we use the Lorentz–Berthelot rules $\sigma_{\text{sw}} = (\sigma_{\text{ss}} + \sigma_{\text{ww}})/2$ and $\epsilon_{\text{sw}} = \sqrt{\epsilon_{\text{ss}}\epsilon_{\text{ww}}}$. Here, $\epsilon_{\text{ww}} = 0.05$ and $\sigma_{\text{ww}} = 1.04/2^{1/6}$ are the parameters for water–water interaction as given in Ref. 28. To increase the efficiency of the simulations, we use a distance cut-off of $3R_{\text{HB}}$ when computing energies. To avoid artifacts due to this cut-off, all Lennard-Jones potentials are shifted to zero at this cut-off.^{41–43}

A Monte Carlo step consists of displacing the center of mass and the orientation of particles randomly by at most R_{max} and 0.125 rad, respectively. The maximum translational displacement, R_{max} , is chosen such as to give an acceptance ratio of 50%. Periodic boundary conditions are used and at every five Monte Carlo sweeps, an attempt to rescale the size of the box is made (one Monte Carlo sweep is equivalent to

$N = 512$ attempted steps). To obtain reliable data, the initial configurations were chosen randomly and the systems were equilibrated at a given temperature for 15×10^4 sweeps. Then, data were gathered over 1×10^7 sweeps. This protocol was repeated for ten samples for each of the temperatures.

The radial distribution function $g(r)$ computed during the simulation is used to estimate the potential of mean force $\text{PMF}(r)$ for the association of solutes. $\text{PMF}(r)$ corresponds to the free energy required to bring two particles from an infinite separation to a distance r ,

$$\text{PMF}(r) = -k_B T \ln(g(r)). \quad (2)$$

The entropy ΔS required to bring a solute from an infinite distance to a distance r is

$$\Delta S(r) = - \left(\frac{\partial \text{PMF}(r)}{\partial T} \right) = - \frac{\text{PMF}_{T+\Delta T}(r) - \text{PMF}_T(r)}{\Delta T}. \quad (3)$$

Using Eqs. (2) and (3), the enthalpy difference $\Delta H(r)$ in this process is

$$\Delta H(r) = \text{PMF}(r) + T \Delta S(r). \quad (4)$$

We also compute the heat capacity of hydration from the potential of mean force as

$$\begin{aligned} \Delta C_p(T) &= -T \left(\frac{\partial^2 \text{PMF}_T(r)}{\partial^2 T} \right)_p \\ &= -T \frac{\text{PMF}_{T+\Delta T}(r) - 2\text{PMF}_T(r) + \text{PMF}_{T-\Delta T}(r)}{(\Delta T)^2}. \end{aligned} \quad (5)$$

To better quantify the role of water in the hydrophobic effect, the number density of MB particles $\rho(r, z)$ around a pair of solutes is computed in polar coordinates during each simulation. The z -axis is defined along the line connecting the centers of mass of the two solute molecules. The zero of this axis is at the midpoint of the line. The r coordinate of a point corresponds to its shortest distance to the z -axis. Taking advantage of the angular invariance around the z -axis, we compute

$$\rho(r, z) = \frac{N(r, z)}{2\pi r dr dz \rho_o}, \quad (6)$$

where $N(r, z)$ is the number of MB molecules at position (r, z) and $\rho_o = N_{\text{water}}/V$. This normalization ensures that $\rho(r, z) \rightarrow 1$ when the distance between a solute and an MB particle approaches infinity.

III. RADIAL DISTRIBUTION FUNCTION

Water molecules in the vicinity of nonpolar solutes are more ordered than bulk water.⁴⁴ An idealization of this ordering is the dodecahedral cage of a crystalline methane hydrate in which the number of water molecules hydrating the solute is 20—see Fig. 1. This ordering of water around isolated solutes has an unfavorable low entropy which can be made more favorable by bringing solutes close to each other. Thus, the formation of contact between solutes decreases the

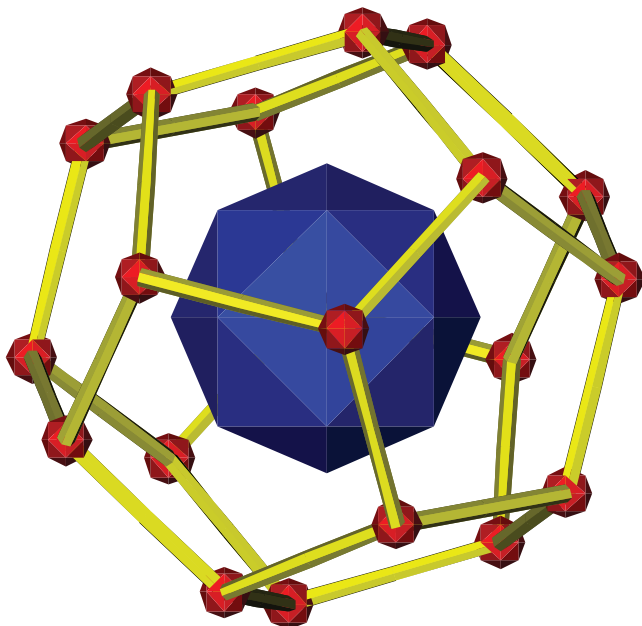


FIG. 1. Schematic representation of a clathrate cage around a hydrophobic particle.

solute–water surface area and, hence, decreases the amount of ordered water molecules. Because of the consequent increase in entropy, contact configurations (CCs) are said to be entropically favorable and they will be studied here using the RDF and the potential of mean force.

Figure 2(a) shows the solute–solute RDF at $T = 0.140$, and Figs. 2(b)–2(d) show the normalized number density of water $\rho(r, z)$ at the peaks and valleys of the RDF.

The first peak corresponds approximately to the solute van der Waals distance ($2^{1/6}\sigma_{ss}$). In this case, the region between solutes is depleted of water as Fig. 2(b) shows.

When the solute molecules are separated by a distance that corresponds to the second peak, the region between them accommodates one layer of water; the position of the second peak corresponds to twice the equilibrium distance between solute and water, i.e., $d_{\text{second peak}} = 2(2^{1/6}\sigma_{sw})$. The presence of water molecules between the two solutes is shown Fig. 2(d). Due to their importance for the hydrophobic effect, atomic configurations at the first and second peaks of the RDF have been assigned specific names *contact configurations* and *solvent separated configurations* (SSCs), respectively. These refer to the absence and presence of water in the region between solute molecules. Configurations at the valley of the RDF are named *desolvation configurations* (DCs). The number density of water at the DC state is shown in Fig. 2(c). There is some evidence that this state plays an important role in the kinetics of protein folding.^{45,46}

The hydrophobic interaction is attractive for small apolar solutes^{2,36} and correlates with their surface area of exposure to water.⁴⁷ Within the RDF, changes in surface area occur when particles undergo transitions into SSC and CC states. Thus, the hydrophobic interaction affects mostly the relative population of these states. Figure 3 shows the temperature dependence of the RDF. In a typical liquid, the molecules become less correlated when heated up. For hydrophobic solutes, however, the population of CC states increases upon heating: solute particles become more correlated at short distances when temperature increases, i.e., their solubility decreases upon increasing temperature. This is shown in Fig. 3. The other states of the system, i.e., SSC and DC, behave as in a typical liquid: the SSC increases while the

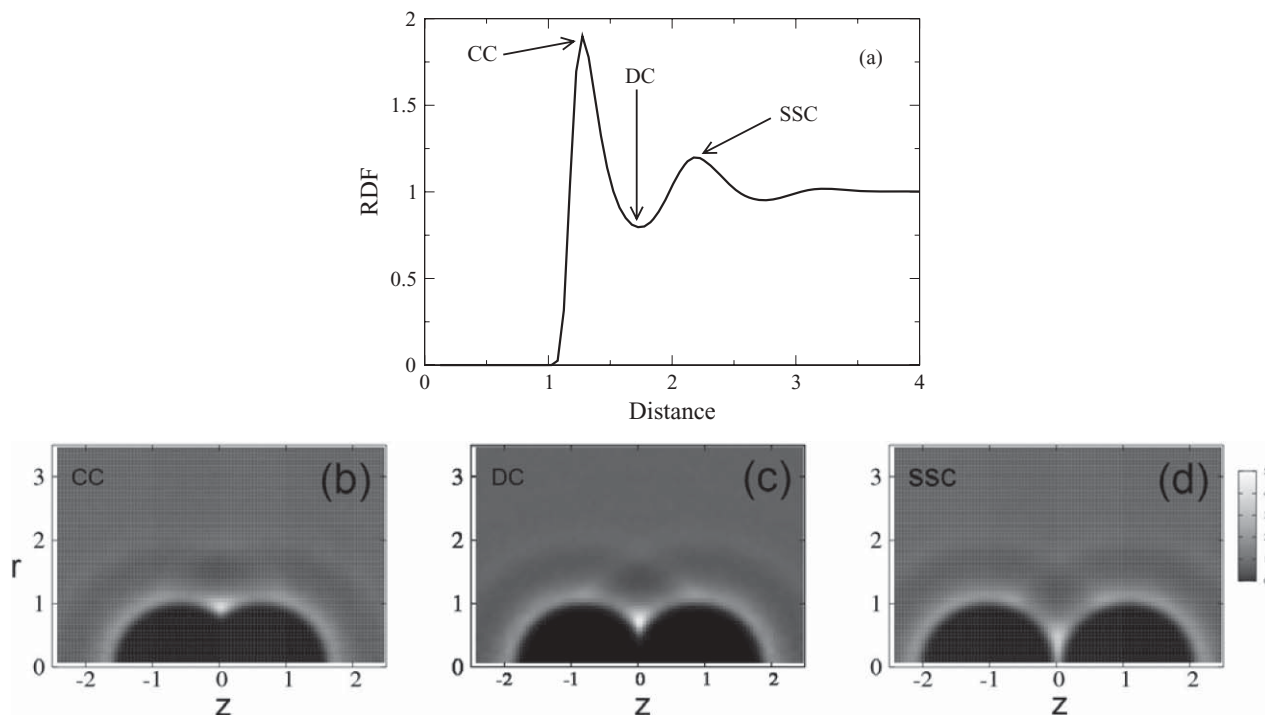


FIG. 2. (a) Solute–solute RDF at $T = 0.140$. (b)–(d) Number density of water molecules around solutes for relevant peaks and valley of the RDF.

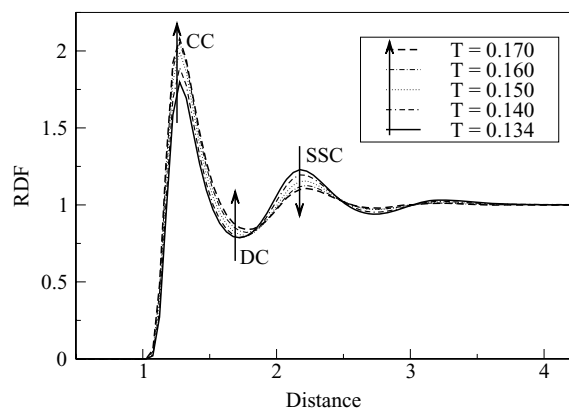


FIG. 3. Temperature dependence of the solute-solute RDF. Arrows indicate changes in the RDF with increasing temperature.

DC decreases upon cooling the system. This observed temperature dependent behavior for CC, DC, and SSC states is in agreement with atomistic simulations using the TIP5P,^{22,48} TIP4P,^{48,49} TIP3P,⁴⁸ SPCE,^{22,48} SPC,⁴⁸ and the two-dimensional MB (Ref. 24) models for water.

To understand this nonintuitive temperature dependent behavior of the hydrophobic effect, in Sec. IV we study the potential of mean force between nonpolar solutes and its decomposition in entropy and enthalpy.

IV. POTENTIAL OF MEAN FORCE

Figure 4 shows the potential of mean force $PMF(r)$, entropic energy $-T\Delta S$, and enthalpy ΔH at $T = 0.140$. These quantities were computed according to Eqs. (2)–(4). Each peak of the RDF corresponds to a minimum in $PMF(r)$. Thus, the first minimum of $PMF(r)$ corresponds to the CC state and the second minimum to the SSC state, as indicated in Fig. 4. $PMF(r)$ corresponds to the free energy required to bring particles from an infinite separation to a distance (r). Subtracting the solute-solute pair potential [Eq. (1)] from $PMF(r)$ yields the solvent mediated contribution to the solute-solute interaction. This contribution is purely attractive for small distances implying that in the absence of solvent, i.e., in the gas phase,

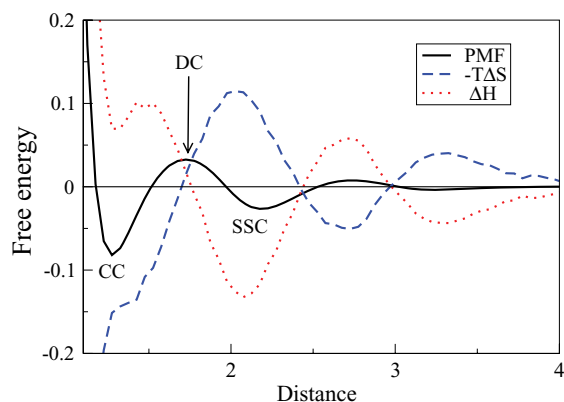


FIG. 4. Potential of mean force (full line), entropic energy (dashed line), and enthalpy (dotted line) of nonpolar solutes at $T = 0.140$.

TABLE I. Number and energy of water in different shell states (ISC, SSC, and CC) and bulk state. These simulations were carried out with two solutes in 610 MB molecules at $T = 0.140$ and $P = 0.20$. ISC: isolated solute configurations, SSC: solvent separated configurations, CC: contact configurations.

State	Number of shell water	Energy
ISC	27	-0.984756
SSC	25	-0.99204
CC	21	-0.987301
Bulk	—	-0.945207

the equilibrium distance between solutes is larger than in the liquid phase.^{55,56}

Within the classical picture of the hydrophobic effect by Frank and Evans,¹⁶ the main energetic change when hydrophobic particles are brought close to each other is given by the transfer of shell water into the bulk as the hydration shell around the solutes overlap. Since shell water is more ordered, this transfer increases the entropy and enthalpy of the system.^{5,8,14,16,35,37} This is in line with the energetic partition of the CC state shown in Fig. 4. This state is entropically stabilized and enthalpically destabilized. On the other hand, when hydrophobic solutes are brought to distances corresponding to the SSC state, the energetics of the system is dominated by enthalpy instead of entropy. This occurs because only a small number of shell water is transferred to the bulk during the formation of the SSC state. Thus, the main mechanism accounting for the relaxation of SSC is the rearrangement of shell water into a lower energetic state.

In other words, from a microscopic point of view, the CC state is characterized by the transfer of shell water into the bulk while this transfer is not the dominant phenomena accounting for the SSC state. To quantify this statement we show in Table I the number of water molecules involved in the hydration of two solutes when these are in the CC, SSC, and ISC (isolated solvent configuration) states. Solute are considered to be isolated, i.e., in the ISC state, when the distance between them is in the range [3.00:3.25]. Note that the absolute number of water molecules involved in hydration depends on the definitions used in the calculation.⁵¹ Simulations and theory computed the average number of water molecules in the first hydration shell around methane solutes. Numbers varied between 14 and 22 water molecules depending on the model and theory used,^{40,52–54} while experiments measured hydration shells with 16, 19, or 20 water molecules.^{55–57}

From Table I, we can conclude that when solutes form the SSC state, i.e., $ISC \rightarrow SSC$, on average two shell water molecules are transferred to the bulk. This is a small number compared to the six shell water molecules that are transferred to the bulk during the formation of the CC state, i.e., when $ISC \rightarrow CC$.

The PMF (Fig. 4) shows that SSC state is characterized by enthalpy minimization which can be explained microscopically by a rearrangement of shell water molecules into lower energetic states. To quantify this statement, we show in Table I the potential energy of a water molecule in the different shell states (ISC, SSC, and CC) and in the bulk state. An energetic penalty of about 0.039 (in units of ϵ_{HB}) is associ-

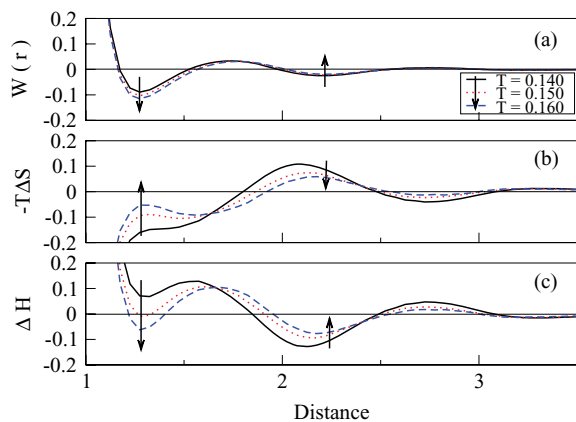


FIG. 5. Potential of mean force (a), entropic energy (b), and enthalpy (c) of nonpolar solutes at different temperatures. Arrows indicate changes in this quantities with increasing temperature at CC and SSC states.

ated with the transfer of one shell water into bulk. There is an energetic gain of -0.007284 when one shell water in the ISC state is transformed into a shell water in the SSC state and a gain of -0.002545 upon transformation into the CC state. Thus, the balance in potential energy for forming SSC and CC states is -0.1041 and $+0.18$, respectively. This shows that the stabilization of the SSC state can be explained by a favorable rearrangement of shell water, while enthalpy cannot explain the stability of CC states. Entropy is required for the stability of CC states, as described above.

V. TEMPERATURE DEPENDENCE

Figure 5(a) shows the PMF, obtained using Eq. (2), at three temperatures. It shows that the attraction well at the CC state becomes deeper and therefore more stable as temperature increases. This unusual behavior is opposite to what happens with standard interactions. For example, for a H-bond the attraction well becomes less pronounced with increasing temperature. The depth of the potential well of the SSC state shows a small, but systematic increase with temperature, as seen in Fig. 5(a).

Figures 5(b) and 5(c) show the entropic energy ($-T\Delta S$) and enthalpy, respectively. At the CC state, the entropic energy increases with increasing temperature contributing to a weakening of the CC state. On the other hand, ΔH decreases and contributes to a stronger CC state. Therefore, *the change in enthalpy when nonpolar solutes are buried at a higher temperature is responsible for the strengthening of the hydrophobic effect*—not the change in entropy. Furthermore, for this phenomenon to occur, the change in enthalpy with increasing temperature has to be higher than the change in the entropic energy. This can be shown analytically from the definitions of the heat capacity,

$$\Delta C_p^{\text{CC}} \equiv d\Delta H^{\text{CC}}/dT = Td\Delta S^{\text{CC}}/dT. \quad (7)$$

First, we obtain the temperature dependence of entropic energy and enthalpy by integrating the equations above using T_s as a starting temperature—defined when $\Delta S^{\text{CC}}(T_s) = 0$,

$$-T\Delta S^{\text{CC}}(T) = -T\Delta C_p^{\text{CC}} \ln\left(\frac{T}{T_s}\right), \quad (8)$$

and

$$\Delta H^{\text{CC}}(T) = \Delta H^{\text{CC}}(T_s) + (T - T_s)\Delta C_p^{\text{CC}}. \quad (9)$$

Second, we compute how these quantities change with respect to temperature,

$$d(-T\Delta S^{\text{CC}}) = -\left[\Delta C_p^{\text{CC}} \ln\left(\frac{T}{T_s}\right) + \Delta C_p^{\text{CC}}\right]dT \quad (10)$$

and

$$d(\Delta H^{\text{CC}}) = \Delta C_p^{\text{CC}}dT. \quad (11)$$

Since $\Delta C^{\text{CC}} < 0$ (see Sec. VI), then $d(\Delta H^{\text{CC}}) < 0$ and the entropic energy is positive, $d(-T\Delta S^{\text{CC}}) > 0$, for temperatures in the range $T_s/e < T < T_s$, where $e = 2.71828$. Since experimentally $T_s \approx 386$ K,⁵⁸ the entropic energy is positive in the whole liquid range of water. These signs for changes in entropic energy and enthalpy are in agreement with the arrows shown in Figs. 5(b) and 5(c). Now, using Eqs. (10) and (11), the amplitude of changes in enthalpy versus entropic energy is

$$\left|\frac{d\Delta H^{\text{CC}}}{d(-T\Delta S^{\text{CC}})}\right| = \left|\frac{1}{-1 - \ln\left(\frac{T}{T_s}\right)}\right| > 1, \quad (12)$$

where the inequality is valid for $T_s/e < T < T_s$. Thus, changes in enthalpy dominate over the respective change in entropic energy and account for the strengthening of the hydrophobic effect with increasing temperature.

Changes at the SSC state with increasing temperature have an opposite direction compared to the CC state—see Fig. 5. These changes are much smaller than changes at the CC state. They are characterized by an increasing enthalpy and decreasing entropic energy ($-T\Delta S$) with increasing temperature. This behavior is consistent with $\Delta C_p(\text{at SSC}) > 0$ (see Sec. VI). Based on Eq. (12), we can also conclude that enthalpic changes are more important in magnitude and therefore are responsible for the weakening of the SSC state with increasing temperature.

VI. HEAT CAPACITY

In addition to a high positive free energy of hydration which is dominated by entropy, the hydrophobic effect also stands out for its high positive heat capacity of hydration.⁵⁹ Accordingly, when hydrophobic solutes are brought into contact, the amount of hydration decreases and the observed change in heat capacity is negative. Figure 6 shows the difference in heat capacity $\Delta C(r)$ measured when solutes are brought from an infinite distance to a distance r at temperature $T = 0.140$. This quantity is computed using Eq. (5). A negative (positive) value of $\Delta C(r)$ means that less (more) energy is required to increase the temperature of the system when solutes are at distance r compared to isolated solutes.

Figure 6 shows that the CC state has a negative heat capacity when compared to isolated solutes. This is related to the transfer of about six shell water molecules (see Table I)—more ordered and stronger bond forming—to the

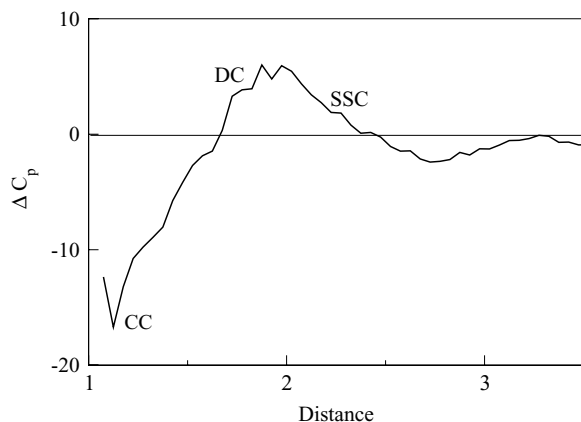


FIG. 6. Dependence of the heat capacity on distance at $T = 0.140$.

bulk. On the other hand, the SSC state has a positive heat capacity as compared to isolated solutes. This is related to the favorable rearrangements of shell water in SSC states.

VII. MICROSCOPIC MECHANISM

In this section, we provide a qualitative microscopic description of the thermodynamic features behind the hydrophobic effect. At the CC state, the main contribution to ΔH and ΔS comes from the transfer of shell water into bulk—see Table I. Within this approximation, at T_s where $\Delta S(T_s) = 0$ the number of microstates that shell and bulk water can assume is the same. This implies that similar to bulk water, shell water has no preferred orientation at T_s , such that in many of these orientations it has at least one H-bond arm pointing toward the solute. Since this dangling arm cannot form a H-bond, many of the microstates of shell water at T_s have a higher energy than the microstates of bulk water; and this implies that $\Delta H(T_s) < 0$.

At temperatures below T_s , the entropy of shell water is smaller than the entropy of bulk water, i.e., $-T\Delta S < 0$. This results from the constraint imposed by the formation of H-bonds. When the strength of these H-bonds is strong enough, it is not possible to fully rotate a water molecule without overlapping its bonding neighbors with the solute or without breaking H-bonds. Thus, the phase space probed by these molecules is smaller than the phase space of bulk water. This explains why the entropic energy is negative below T_s . As the strength of H-bonds increases with decreasing temperature, the difference in allowed states between shell and bulk water increases and $-T\Delta S(T)$ decreases, as shown in Fig. 5(b) for the CC state.

Configurations in which shell water has one of its H-bond arms pointing away from the solute are consistent with the constraint imposed by the formation of H-bonds. Figure 1 is a schematic representation of a clathrate cage, where all the water molecules surrounding the solute have one H-bond arm pointing away from the solute. While a complete closed cage is not likely to form in water, the population of individual shell water in these clathrate configurations increases as temperature decreases. In these configurations, the other three arms of the molecule form angles of about 60° with the sur-

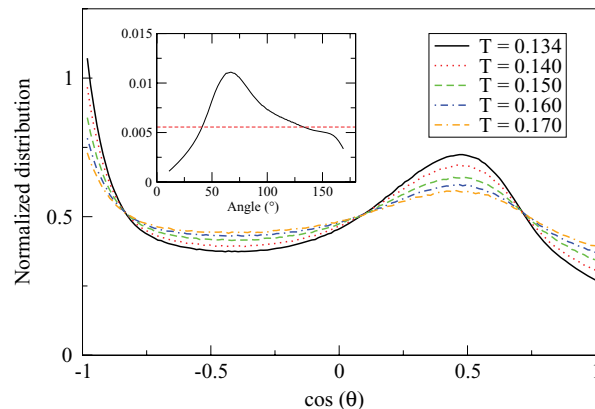


FIG. 7. Normalized distribution of the orientation of shell water at different temperatures as a function of $\cos(\theta)$. (Inset) Distribution of the orientation of shell water as a function of θ for $T = 0.140$ (full line) compared to a random distribution of water orientation (dashed line).

face. As such, the population of H-bond arms in the first shell around the solute increases by a factor of 3 every time one of these configurations is formed. This high concentration of H-bond arms at the surface of the solute favors the formation of strong H-bonds. Thus, as temperature decreases, the enthalpy of shell water decreases faster than that of the bulk water. As a consequence, ΔH , which is negative at T_s , increases with decreasing temperature. It becomes zero at T_h , with $T_h < T_s$, and keeps increasing as the temperature is reduced below T_h . This enthalpic behavior is visible in Fig. 5(c) for the CC state.

The increase in clathrate configurations of water as temperature decreases is quantified in Fig. 7. This figure shows the temperature dependence of shell water orientation distribution. The orientation is defined by the cosine of the angle between the H-bond arm and the distance vector between the MB particle and the solute. Thus, $\cos(\theta) = -1$ occurs when one arm points away from the solute and $\cos(\theta) = 1$ when it points toward the solute. At $\cos(\theta) = 0.5$, the H-bond arm forms an angle of 60° with the surface. At a higher temperature, e.g., $T = 0.17$, this angular distribution becomes almost flat, favoring only slightly configurations with one arm pointing away from the surface. As temperature decreases, the bias in favor of these “clathrate” configurations increases and the distribution peaks strongly at $\cos(\theta) = 0.5$ while many configurations are found with $\cos(\theta) = -1$ as opposed to $\cos(\theta) = 1$. Similar distribution has been obtained for TIP3P.⁶⁰ In the inset of Fig. 7, we show the same distribution but now as function of the angle θ for $T = 0.140$ (full line) and compare it to a random distribution of water orientation (dashed line). Water configurations with one arm pointing toward the solute ($\theta = 0^\circ$) are clearly disfavored, while configurations with $\theta = 60^\circ$ occur with a strong probability. Also, configurations where arms pointing away from the solute ($\theta > 90^\circ$) are very likely to occur.

To understand the negative heat capacity of association at the CC state (see Fig. 6), we use Eq. (7). According to this equation, a negative heat capacity of association occurs either if ΔH decreases with increasing temperature or if $-T\Delta S$ increases with increasing temperature. As described above, these temperature dependencies are explained by a decrease

in the number of clathrate configurations of water molecules as temperature increases.

VIII. DISCUSSION AND CONCLUSION

In this paper, we study the temperature dependence of the hydrophobic effect using the 3DMB model of water. We show that this recently proposed model accounts for different features of the hydrophobic interaction. At the molecular level, hydrophobic particles can be found in equilibrium in two different states: CCs and SSCs. The latter occurs when the van der Waals spheres of the solutes touch each other and the former occurs when one layer of water molecules separates the different solutes. These two equilibrium states are separated by an energetic barrier: the desolvation barrier.

For small solutes comparable to argon and methane, the energy of CC states results from the transfer of about six shell water to the bulk—see Table I. These shell water form cage-like configurations (see Fig. 1), which at low temperatures are enthalpically favorable and entropically unfavorable. Thus, when hydrophobic solutes are brought into contact, less water molecules are in cage-like configurations and this accounts for a larger entropy and larger enthalpy. Since the reduction in entropic energy ($-T\Delta S$) is larger than the increase in enthalpy, the CC state corresponds to an energetically favorable configuration.

As temperature decreases the formation of cage-like configurations by individual shell water molecules increases—see Fig. 7. Accordingly, the entropic energy of transfer increases with increasing temperature. However, this destabilizing effect is overcompensated for by a reduction in the enthalpy of transfer, which explains the strengthening of hydrophobic interaction with increasing temperature. While the free energy resulting from this enthalpic/entropic compensation is small,⁶¹ it has a strong implication for the stability of biological molecules leading to cold denaturation in proteins.^{8,39,62}

While the formation of the CC state is accounted for by the transfer of six shell water molecules to the bulk, the energy of the SSC state is characterized by a rearrangement of the H-bond network of shell water into low energetic states. Accordingly, the SSC state is enthalpically stabilized and since H-bonds become weaker as temperature increases, the favorable enthalpic SSC state becomes less favorable with increasing temperature.

As a word of caution we should mention that an assessment of free energies of hydration require accurate models for water. In particular, an accurate dependence of the density on temperature $(\partial\rho/\partial T)_P$ is needed to account properly for the enthalpy of hydration,

$$\Delta H = -kT^2 \left(\frac{\partial G/kT}{\partial T} \right)_P. \quad (13)$$

This can be seen by dividing ΔH in constant-density and density-dependent terms,

$$\Delta H = -kT^2 \left(\frac{\partial G/kT}{\partial T} \right)_\rho - kT^2 \left(\frac{\partial G/kT}{\partial \rho} \right)_T \left(\frac{\partial \rho}{\partial T} \right)_P. \quad (14)$$

Ikeguchi *et al.*⁶³ have shown that for small cavities in water, $((\partial\Delta G/kT)/\partial T)_\rho$ is small and positive, while $((\partial\Delta G/kT)/\partial\rho)_T$ has little dependence on density and temperature. Thus, the temperature dependence of ΔH is mainly due to $(\partial\rho/\partial T)_P$.^{63–65} The 3DMB model reproduces qualitatively the dependence of density on temperature for water²⁸ and therefore can be used to describe qualitatively the enthalpic–entropic compensation of hydrophobic hydration. We should also mention that the large number of solutes (eight solutes) used here and required to obtain precise values for the RDF (Refs. 22, 41, 66, and 67) implies that our PMFs might have been affected by the presence of nearby solutes. However, the qualitative aspects of the PMF as well as the temperature dependence of the enthalpic–entropic compensation discussed here are in agreement with previous work.^{21,25,26,48,50}

In summary, we used the three-dimensional Mercedes-Benz model for water and Monte Carlo simulations to study the structure and thermodynamics of the hydrophobic interaction. Radial distribution functions are used to classify different cases of the interaction, namely contact configurations, solvent separated configurations, and desolvation configurations. The temperature dependence of these cases is shown to be in qualitative agreement with atomistic models of water. In particular, while the energy for the formation of contact configurations is favored by entropy, its strengthening with increasing temperature is accounted for by enthalpy. This is consistent with our simulated heat capacity. An important feature of the model is that it can be used to account for well-converged thermodynamics quantities, e.g., the heat capacity of transfer. Microscopic mechanisms for the temperature dependence of the hydrophobic interaction are discussed at the molecular level based on the conceptual simplicity of the model.

ACKNOWLEDGMENTS

C.L.D. would like to thank Jirasak Wong-ekkabut for helping with Fig. 1. The work of M.K. was supported by the Natural Sciences and Engineering Research Council of Canada (M.K.) and of T.A.N. and M.K. by the Academy of Finland through its COMP CoE and TransPoly grants. Computational resources were provided by SharcNet [www.sharcnet.ca].

¹C. Tanford, *Science* **200**, 1012 (1978).

²D. Chandler, *Nature (London)* **437**, 640 (2005).

³M. Jensen and O. G. Mouritsen, *Biochim. Biophys. Acta* **1666**, 205 (2006).

⁴R. Zhou, X. Huang, C. J. Margulis, and B. J. Berne, *Science* **305**, 1605 (2004).

⁵C. L. Dias, T. Ala-Nissila, J. Wong-ekkabut, I. Vattulainen, M. Grant, and M. Karttunen, *Cryobiology* **60**, 91 (2010).

⁶P. De Los Rios and G. Caldarelli, *Phys. Rev. E* **63**, 031802 (2001).

⁷P. D. L. Rios and G. Caldarelli, *Phys. Rev. E* **62**, 8449 (2000).

⁸W. Kauzmann, *Adv. Protein Chem.* **14**, 1 (1959).

⁹K. A. Dill, *Biochemistry* **29**, 7133 (1990).

¹⁰P. R. Wolde, *J. Phys. Condens. Matter* **14**, 9445 (2002).

¹¹G. Hummer, S. Garde, A. E. García, and L. R. Pratt, *Chem. Phys.* **258**, 349 (2000).

¹²E. E. Meyer, K. J. Rosenberg, and J. Israelachvili, *Proc. Natl. Acad. Sci. U.S.A.* **103**, 15739 (2006).

- ¹³B. Widom, P. Bhimalapuram, and K. Koga, *Phys. Chem. Chem. Phys.* **5**, 3085 (2003).
- ¹⁴N. T. Southall, K. A. Dill, and A. D. J. Haymet, *J. Phys. Chem. B* **106**, 521 (2002).
- ¹⁵C. Tanford, *Protein Sci.* **6**, 1358 (1997).
- ¹⁶H. S. Frank and M. W. Evans, *J. Chem. Phys.* **13**, 507 (1945).
- ¹⁷C. L. Dias, T. Ala-Nissila, J. Wong-ekkabut, I. Vattulainen, M. Grant, and M. Karttunen, *Cryobiology* **60**, 356 (2010).
- ¹⁸D. T. Bowron, A. Filippini, M. A. Roberts, and J. L. Finney, *Phys. Rev. Lett.* **81**, 4164 (1998).
- ¹⁹Y. Rezus and H. Bakker, *Phys. Rev. Lett.* **99**, 148301 (2007).
- ²⁰L. R. Pratt and D. Chandler, *J. Chem. Phys.* **67**, 3683 (1977).
- ²¹S. Shimizu and H. S. Chan, *J. Am. Chem. Soc.* **123**, 2083 (2001).
- ²²D. Paschek, *J. Chem. Phys.* **120**, 10605 (2004).
- ²³M. S. Moghaddam, S. Shimizu, and H. S. Chan, *J. Am. Chem. Soc.* **127**, 303 (2005).
- ²⁴N. T. Southall and K. A. Dill, *Biophys. Chem.* **101–102**, 295 (2002).
- ²⁵S. Shimizu and H. S. Chan, *J. Chem. Phys.* **115**, 1414 (2001).
- ²⁶S. Shimizu and H. S. Chan, *Proteins: Struct., Funct., Bioinf.* **48**, 15 (2002).
- ²⁷T. Ghosh, A. E. Garca, and S. Garde, *J. Phys. Chem. B* **107**, 612 (2003).
- ²⁸C. L. Dias, T. Ala-Nissila, M. Grant, and M. Karttunen, *J. Chem. Phys.* **131**, 54505 (2009).
- ²⁹A. Ben-Naim, *J. Chem. Phys.* **54**, 3682 (1971).
- ³⁰A. Ben-Naim, *Water and Aqueous Solutions* (Plenum Press, New York, 1974).
- ³¹A. Ben-Naim, *Molecular Theory of Water and Aqueous Solutions*, 1st ed. (World Scientific, Singapore, 2009).
- ³²A. Bizjak, T. Urbic, V. Vlachy, and K. Dill, *Acta Chim. Slov.* **54**, 532 (2007).
- ³³A. Bizjak, T. Urbic, V. Vlachy, and K. A. Dill, *J. Chem. Phys.* **131**, 194504 (2009).
- ³⁴T. Hynninen, V. Heinonen, C. L. Dias, M. Karttunen, A. S. Foster, and T. Ala-Nissila, *Phys. Rev. Lett.* **105**, 086102 (2010).
- ³⁵K. A. T. Silverstein, A. D. J. Haymet, and K. A. Dill, *J. Am. Chem. Soc.* **120**(13), 3166 (1998).
- ³⁶N. T. Southall and K. A. Dill, *J. Phys. Chem. B* **104**, 1326 (2000).
- ³⁷K. A. Dill, T. M. Truskett, V. Vlachy, and B. Hribar-Lee, *Annu. Rev. Biophys. Biomol. Struct.* **34**, 173 (2005).
- ³⁸J.-P. Becker and O. Collet, *J. Mol. Struct.: THEOCHEM* **774**, 23 (2006).
- ³⁹C. L. Dias, T. Ala-Nissila, M. Karttunen, I. Vattulainen, and M. Grant, *Phys. Rev. Lett.* **100**, 118101 (2008).
- ⁴⁰S. F. Dec, S. J. Gill, *J. Solution Chem.* **14**, 417 (1985).
- ⁴¹M. P. Allen and D. J. Tildesley, *Computer Simulation of Liquids* (Oxford University Press, New York, 1987).
- ⁴²D. J. Bonhuis, D. Horinek, L. Bocquet, and R. R. Netz, *Phys. Rev. Lett.* **103**, 144503 (2009).
- ⁴³J. Wong-ekkabut, M. S. Miettinen, C. Dias, and M. Karttunen, *Nat. Nanotechnol.* **5**, 555 (2010).
- ⁴⁴E. Sobolewski, M. Makowski, C. Czaplowski, A. Liwo, S. Odziej, and H. A. Scheraga, *J. Phys. Chem. B* **111**, 10765 (2007).
- ⁴⁵M. S. Cheung, A. E. Garca, and J. N. Onuchic, *Proc. Natl. Acad. Sci. U.S.A.* **99**, 685 (2002).
- ⁴⁶Z. Liu and H. S. Chan, *J. Mol. Biol.* **349**, 872 (2005).
- ⁴⁷B. Lee and F. M. Richards, *J. Mol. Biol.* **55**, 379 (1971).
- ⁴⁸D. Paschek, *J. Chem. Phys.* **120**, 6674 (2004).
- ⁴⁹S. Shimizu and H. S. Chan, *J. Chem. Phys.* **113**, 4683 (2000).
- ⁵⁰D. E. Smith and A. D. J. Haymet, *J. Chem. Phys.* **98**, 6445 (1993).
- ⁵¹Solutes are considered to be in the CC state if the distance between them is smaller than 1.65—this corresponds to the first minimum in the solute–solute RDF. The SSC state is defined when the distance between solutes is within [1.65:2.73]. Water is considered to form a shell around the solute if their distance to the solute is smaller than 1.65—this corresponds to the first minimum of the water–solute RDF.
- ⁵²S. J. Gill, S. F. Dec, G. Olofsson, and I. Wadso, *J. Phys. Chem.* **89**, 3758 (1985).
- ⁵³J. H. Griffith and H. A. Scheraga, *THEOCHEM* **682**, 97 (2004).
- ⁵⁴S. Swaminathan, S. W. Harrison, and D. L. Beveridge, *J. Am. Chem. Soc.* **100**, 5705 (1978).
- ⁵⁵C. A. Koh, R. P. Wisbey, X. Wu, R. E. Westacott, and A. K. Soper, *J. Chem. Phys.* **113**, 6390 (2000).
- ⁵⁶P. H. K. De Jong, J. E. Wilson, G. W. Neilson, and A. D. Buckingham, *Mol. Phys.* **91**, 99 (1997).
- ⁵⁷S. F. Dec, K. E. Bowler, L. L. Stadterman, C. A. Koh, and E. Dendy Sloan, Jr., *J. Am. Chem. Soc.* **128**, 414 (2006).
- ⁵⁸R. L. Baldwin, *Proc. Natl. Acad. Sci. U.S.A.* **83**, 8069 (1986).
- ⁵⁹J. T. Edsall, *J. Am. Chem. Soc.* **54**, 1506 (1935).
- ⁶⁰N. Tsunekawa, H. Miyagawa, K. Kitamura, and Y. Hiwatari, *J. Chem. Phys.* **116**, 6725 (2002).
- ⁶¹T. Yoshidome and M. Kinoshita, *Phys. Rev. E* **79**, 30905 (2009).
- ⁶²P. L. Privalov, Y. V. Griko, and S. Y. Venyaminov, *J. Mol. Biol.*, **190**, 487 (1986).
- ⁶³M. Ikeguchi, S. Shimizu, S. Nakamura, and K. Shimizu, *J. Phys. Chem. B* **102**, 5891 (1998).
- ⁶⁴B. Lee, *Biopolymers* **24**, 813 (1985).
- ⁶⁵K. J. Soda, *J. Phys. Soc. Jpn.* **62**, 1782 (1993).
- ⁶⁶T. Ghosh, A. E. Garcia, and S. Garde, *J. Chem. Phys.* **116**, 2480 (2002).
- ⁶⁷T. Ghosh, A. E. Garcia, and S. Garde, *J. Am. Chem. Soc.* **123**, 10997 (2001).